# Non-dimensional scaling of passive adaptive blades for a marine current turbine

K. Van Ness, A. Aliseda, and B. Polagye

*Abstract*—**Current turbine blades that passively deform in operation (i.e., passive adaptive blades) are attractive for their load reduction potential in flow conditions that exceed the rated condition, or under unsteady loads. By tailoring the ply angle in a unidirectional carbon fiber blade, a desired twist can can be induced in response to bending of the blade under load. In developing this form of passive adaptive control, a fundamental question is how to non-dimensionalize the fluid-structure interaction to make laboratory-scale experiments relevant to full-scale applications. To address this, we perform a set of Cauchy-scaled experiments using blades with identical bend-twist coupling but different bending stiffness. Blades were tested in a recirculating flume with chord-based Reynolds numbers ranging from $6.9 \cdot 10^4$ to $2.7 \cdot 10^5$ while measuring force and torque on the rotor and blade, which were used to characterize power and thrust and to calculate the span-wise and chord-wise center of pressure on the blade. Simultaneously, a high-speed camera observed *in-situ* deflection and twist at the blade tip. Results demonstrate that the Cauchy number is a meaningful parameter for scaling passive adaptive current turbine blades under hydrodynamic loads, and to model steady-state hydrodynamic and hydroelastic behavior.**

*Index Terms*—**axial-flow current turbine, bend-twist coupling, blade deformation, non-dimensional scaling, passive adaptive blade**

## I. Introduction

WATER currents, driven by gravity, tides, wind, and density differences, carry kinetic power that can be converted by current turbines into electricity. In strong currents, it is sometimes necessary to employ a control strategy to regulate power output at the turbine's "rated power" to avoid blade or generator failure. To hold power constant, efficiency must be precisely decreased as inflow increases, which can be achieved through changes in rotation rate, $\omega$, or blade pitch, $\beta$. Adjustments in blade pitch could be accomplished through an active strategy, using motorized blades, or a passive strategy, using flexible, self-twisting blades, also known as passive adaptive blades.

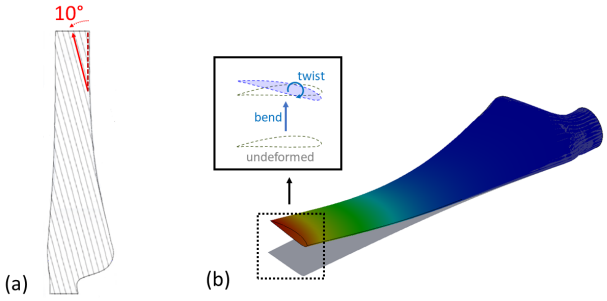


Fig. 1. The self-twisting in a passive adaptive blade can be achieved by using (a) unidirectional, off-axis fibers, which results in anisotropic blade properties and (b) a coupling between flapwise deflection and span-wise twisting.

### A. Passive adaptive blades

Numerical [1]–[4], experimental [5]–[12], and theoretical [13] studies demonstrate the potential advantages of using flexible, passive adaptive blades for load mitigation in above-rated or unsteady flow conditions. By tailoring the off-axis orientation of the composite fibers of the blade, a passive adaptive blade can be designed with a "bend-twist coupling", such that deflection in the flapwise direction is coupled to twisting in the span-wise direction (Fig. 1). When given a positive fiber orientation, the bend-twist coupling allows for passive twisting of the blade towards the feathered position (i.e., decreased angles of attack) to shed power and thrust [1], [4], [5], [7], similar to an active pitch mechanism. Bend-twist coupled blades, or passive adaptive blades, have been researched in wind and propulsion for decades as a means to reduce structural loads [2], [14]–[30]. Conversely, despite the economic benefits of maintenance cost reduction and reliability improvement, passive adaptive blade research for current turbines is more limited.

### B. Cauchy scaling

While dimensionless scaling relations have been extensively studied for current turbines with rigid blades [31], [32], relatively few studies discuss appropriate hydroelastic scaling for flexible blades with tailored off-axis fiber orientations. Extending laboratory results to full-scale, open-water applications requires an understanding of hydrodynamic and hydroelastic scaling to



Funding was provided by the Naval Facilities Engineering Command (NAVFAC) under N00024-10-D-6318 Task Order 0067 and N00024-10-D-6318 Task Order N00024-18-F-8702. This research was also supported in part by an appointment with the Marine and Hydrokinetic Graduate Student Research Program sponsored by the U.S. Department of Energy (DOE), Office of Energy Efficiency and Renewable Energy, and Water Power Technologies Office. This program is administered by the Oak Ridge Institute for Science and Education (ORISE) for the DOE. ORISE is managed by ORAU under DOE contract number DESC0014664. All opinions expressed in this paper are the authors' and do not necessarily reflect the policies and views of DOE, ORAU, or ORISE.

All authors are with the Mechanical Engineering Department, University of Washington, 3900 E Stevens Way NE, Seattle WA 98195 (emails: kvanness@uw.edu, aaliseda@uw.edu, bpolagye@uw.edu).

Digital Object Identifier:
https://doi.org/10.36688/ewtec-2023-231

use the existing data correctly in the design of large systems.

While the body of knowledge for aeroelastic scaling in aircraft applications is vast [33]–[35], this does not translate directly to current turbines because of large differences in the solid-to-fluid density ratio and Reynolds numbers. A relatively small number of prior studies investigate hydroelastic scaling for marine propulsion and lifting bodies [36]–[41] and wind turbine applications [28], [29], [42].

Cauchy similarity is important when modeling a structure with significant elastic forces [36]. We define the Cauchy number, $Ca$, as:

$$Ca = \frac{\rho_f {U_\infty}^2}{E}, \tag{1}$$

where $\rho_f$ is the density of the fluid, $U_\infty$ is the free-stream velocity, and $E$ is the transverse flexural modulus of the blade (i.e., corresponding to bending primarily in the streamwise direction).

The relevant non-dimensional parameters identified by Young [40] that govern elastic marine propulsor performance are: elasticity ratio (equivalent to the Cauchy number), advance coefficient (equivalent to the tip-speed ratio in turbine literature), Froude number, Reynolds number, Mach number, cavitation number, bend-twist coupling, density ratio between the solid and fluid, and ratio of effective bending stiffness to torsional stiffness. While matching Froude, Reynolds, and Mach number cannot be achieved simultaneously, Motley and Young [38] and Young [40] recommend prioritizing Mach scaling in cases where gravitational effects are negligible and the boundary layer is fully turbulent (i.e., where performance is Reynolds-independent). However, this requires matching the free-stream velocity and material properties between the model and full-scale prototypes, which can be difficult or impossible to achieve in many small-scale facilities.

A recent study by Ng *et al.* [41] demonstrates, through a numerical model, that when Cauchy similarity is achieved between model and full-scale, the same steady-state dimensionless loads and deformations are observed across scales, even when the density ratio is not maintained. It is precisely this numerical result that we aim to experimentally demonstrate in this study for a marine current turbine, thereby confirming that scaling with Cauchy number yields similar steady-state blade loading and blade deformations for different flow conditions and blade mechanical properties.

## II. Methods

### A. Blade fabrication

The blade design and fabrication process used in this work is similar to that described in [5]. A thicker root was used to manage an undesirable stress concentration identified by Barber *et al.*, and adjustments to the blade fabrication process were implemented to minimize blade-to-blade variability. The exact blade geometry, based on the NACA-44 airfoil series, is provided in Appendix A.

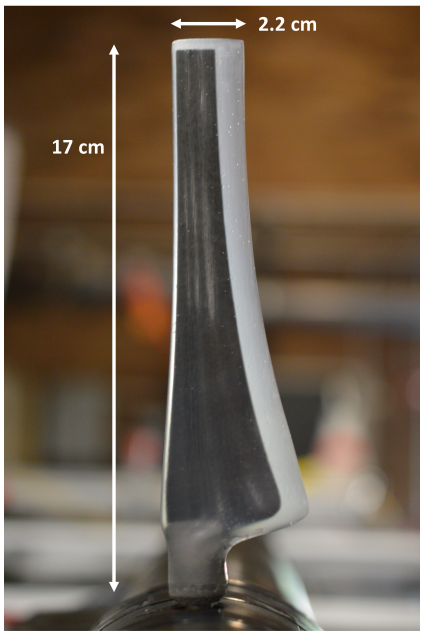


Fig. 2. Flexible, composite blades composed of a carbon fiber spar (black), to provide the desired bend-twist coupling, and a semi-rigid polyurethane outer (translucent white-grey) to provide the desired blade geometry and hydrodynamic behavior.

Since small-scale composite blades can be difficult to fabricate using conventional methods without excessive stiffness and inaccuracies in fiber orientation [5], [43], a nonconventional layup technique was used for these blades. Figure 2 shows the fully fabricated, 17 cm composite blade, consisting of a 5- or 7-ply carbon fiber spar (Hexcel AS4, 12K filament count) which provides the desired bend-twist coupling, cast in a semi-rigid polyurethane (Smooth-cast 45D) which provides the desired hydrofoil cross-section and hydrodynamic behavior. This semi-rigid body allows the material properties of the carbon fiber to dominate the overall mechanical properties of the blade. Two sets of composite, passive adaptive blades with a $10^\circ$ fiber angle orientation were fabricated: one using a 5-ply (1.0 mm thick) spar and one using a 7-ply (1.4 mm thick) spar. A fiber angle orientation of $10^\circ$ was chosen so that the differences in stiffness would be significant while a fiber orientation greater than $10^\circ$ is impractical in most current turbine applications, as the bending stiffness decreases drastically for larger ply angles and blades with large bend-twist couplings may not have favorable performance below rated flow conditions.

To provide a rigid blade reference, a set of aluminum blades matching the unloaded blade geometry of the composite blades were machined. Since 3-4% shrinkage in chord length relative to the mold dimensions was observed during the curing of the polyurethane, the aluminum blade profile was extracted from computerized tomography (CT) scans of the composite blades.

### B. Turbine instrumentation

A 0.45-diameter current turbine, shown in Fig. 3, was used for performance testing. Due to the blade-to-blade variability observed in the in-air static mechanical test-

ing of full blade sets and the need for precise values of bending stiffness and bend-twist coupling to maintain Cauchy number similarity, we used single-bladed tests for this scaling investigation. This allowed us to select one blade from each set that had the closest agreement in bend-twist behavior. Instrumented with six-axis load cells on both the driveshaft (Mini45, ATI Industrial Automation) and blade root (Nano25, ATI Industrial Automation), the blade load cell measurements, sampled at $\approx$ 100 Hz, were used since the loads from a single blade were too small to measure accurately with the driveshaft load cell (Fig. 4). However, we note that due to the positioning of a shaft seal between the blade load cell and the blade root, these load cell measurements underpredict blade loading, as approximately 7% of the blade loads are absorbed by the seal. The turbine rotor is connected to a 5:1 gearbox (PV23, Parker Hannefin) and doubleshaft stepper motor (LV233, Parker Hannifin), with an optical encoder mounted on the shaft. The stepper motor allows for precise control of the rotational speed. Additional details related to data acquisition and temperature management in the nacelle are described in [44].

### C. Experimental facility

Experiments were conducted in the Alice C. Tyler Flume at the University of Washington, a recirculating open-channel flume with a test section 0.6 meter in depth and 0.76 meter in width. This resulted in a blockage ratio (rotor swept area relative to the channel cross-section) of 35%. A constant freestream velocity was achieved using two pumps controlled by a variable frequency drive. Turbulence intensities were relatively low (2.0 and 4.4%) for the two inflow velocities of $0.55$ m/s and $0.80$ m/s used in this study [44]. The freestream velocity, $U_\infty$, was measured 3 diameters upstream of the rotor plane using an acoustic Doppler velocimeter (ADV, Nortek Vector) sampling at 64 Hz. We define the chord-based Reynolds number using the local chord length, $c$, at the 3/4 blade-span point (23.0 mm) as the characteristic length and the approximate relative velocity incident on the blade, neglecting induction, as the characteristic velocity:

$$Re_c = \frac{c\sqrt{{U_\infty}^2 + (\omega r)^2}}{\nu} = \frac{cU_\infty\sqrt{1+\lambda^2}}{\nu}, \qquad (2)$$

where $r$ is the the local turbine radius at the 3/4 blade-span point (182.5 mm), $\nu$ is the kinematic viscosity, and $\lambda$ is the tip-speed ratio, $\lambda = \omega r/U_\infty$. $Re_c$ ranged from $6.9 \cdot 10^4 - 2.7 \cdot 10^5$. Reynolds-independence for this turbine and blade geometry has been previously confirmed for $Re_c > 5 \cdot 10^4$ [44]. Water temperature was maintained at $33°C$ to preserve Reynolds-independence at lower inflow speeds.

### D. Performance Characterization

Turbine performance of each blade type (5- and 7-ply) was characterized as a function of tip-speed ratio, $\lambda$, which was varied by adjusting rotation rate while inflow velocity remained constant. Mechanical power output was calculated from the rotational speed, $\omega$, given by the stepper motor and the torque, $Q_{y,b}$, measured by the six-axis load cell at the blade root, adjusted to account for the distance between the blade load cell and the driveshaft axis of rotation. The resultant power was used to compute the coefficient of performance:

$$C_P = \frac{\langle (Q_{y,b} + F_{x,b}R)\omega \rangle}{0.5\rho_f A \langle {U_\infty}^3 \rangle}, \qquad (3)$$

where $Q_{y,b}$ is the torque on the blade in the streamwise direction, $F_{x,b}$ is the force on the blade in the direction of rotation, $R$ is the distance from the sensor head to the rotor's driveshaft (3.57 cm) (Fig. 4), $A$ is the rotor swept area (undeformed), and $\rho_f$ is the water density. The averages for the mechanical power and kinetic energy flux are calculated separately due to asynchronous clocks. This approximation is acceptable given the low turbulence intensity in the flume. Thrust measured by the blade load cell, $F_{y,b}$, was used to calculate the coefficient of thrust:

$$C_T = \frac{\langle F_{y,b} \rangle}{0.5\rho_f A \langle {U_\infty}^2 \rangle} \qquad (4)$$

Torque and thrust measurements were adjusted by an average of the azimuthally-dependent tare values recorded under zero inflow. At each tip-speed ratio, $C_P$ and $C_T$ were averaged over 9000 samples, or 90-380 revolutions depending on the rotational speed. Averaging over a whole number of rotations was confirmed to be inconsequential when averaging over such a high number of turbine rotations. We considered adapting the calculation of swept area in Eqns. 3 and 4 to account for deflection, but the effect was small compared to other sources of experimental uncertainty. For example, the maximum measured deflection corresponds to a reduction in swept area of 1.4%.

### E. Blade deformation

To improve our understanding of passive adaptive blade deformation during turbine operation, a test was devised to remotely measure the turbine blade's structural response to hydrodynamic loads. A high speed camera (Vision Research, Phantom c641) was positioned below the glass test section of the flume to capture the location and orientation of each passing blade tip (Fig. 5) at a frame rate of at least 700 fps and a resolution of 1024x1024 pixels. Blade tips were coated with a reflective chrome paint to increase contrast. Video of at least 15 blade passages was recorded at each tip-speed ratio. During image processing, the frame that most closely aligns the blade in the center of the camera view was compared to an image of the unloaded blade to calculate deflection and twist at the blade tip. More specifically, each frame was binarized, converting each pixel above or below a given light intensity threshold to white or black, and the centroid and major axis orientation of the white region, identified as the blade tip, were calculated (Fig. 5). The pixel scale was determined by the ratio of the pixel length of the major axis in the reference (i.e., stationary)

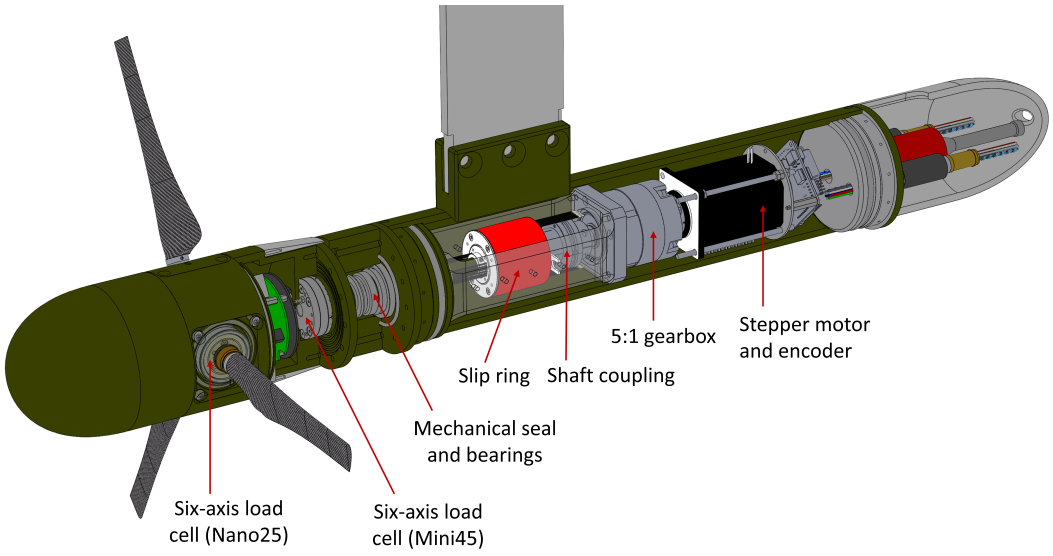


Fig. 3. CAD model of turbine and instrumentation.

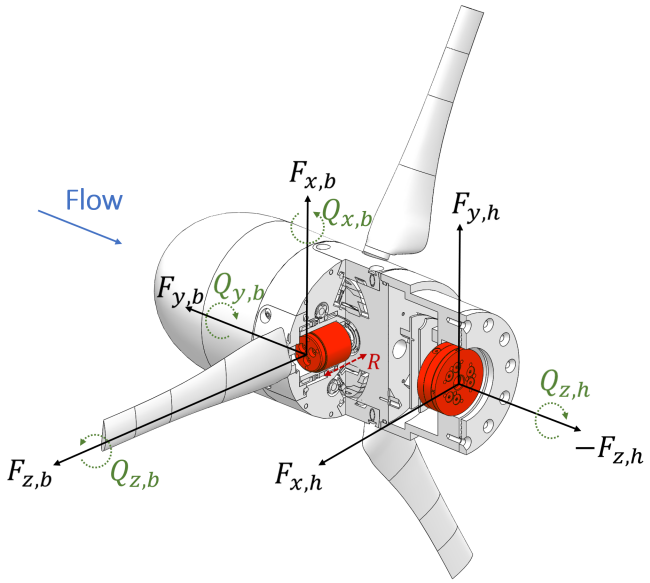


Fig. 4. Blade and driveshaft load cell coordinate systems. Note, the subscripts "b" refer to force/torque components measured by the load cell installed at the blade root while the subscripts "h" refer to force/torque components measured by the load cell installed at the back of the rotor hub on the end of the driveshaft.

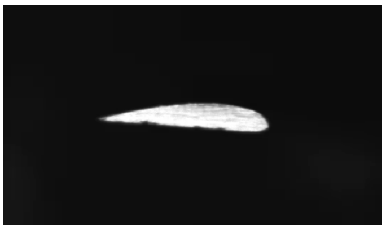

(a)

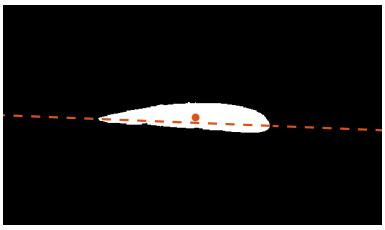

(b)

Fig. 5. High-speed video of the rotor plane during flume testing was used to calculate tip deflection and twist by (a) identifying a high-contrast object as the blade and (b) binarizing the frame to segment the blade tip from the background, then measuring the position of the centroid and orientation of the major axis in order to calculate tip deflection and twist relative to the unloaded blade.

frame to the measured chord length of the physical blade tip. The tip deflection, $\delta$, was determined from the displacement of the centroid, while the tip twist, $\Delta\beta$, was determined from the change in orientation of the major axis, thus fully capturing the coupled deformation shown in Fig. 1.

### F. Cauchy scaling

To understand the effectiveness of Cauchy-scaling in producing similar steady-state performance and blade deformation, we designed two experimental setups with different $E$ and $U_\infty$ that maintained a constant Cauchy number as

$$Ca_A = \frac{\rho_f {U_A}^2}{E_A} = \frac{\rho_f {U_B}^2}{E_B} = Ca_B. \tag{5}$$

The first blade used a 7-ply carbon fiber spar and the second blade used a 5-ply carbon fiber spar, both fabricated with a $10^\circ$ fiber orientation and cast in the same mold to produce identical foil cross-sections. This resulted in two blades with similar bend-twist coupling (Fig. 7(c)), but with differing effective elastic moduli, $E$. While the 7-ply design was an extension of previous work [5], the 5-ply design was selected based on an estimate of bending stiffness matrices for layups of various ply counts using the material properties ($E_1$, $E_2$, $G_{12}$, and $\nu_{12}$) of the carbon fiber listed in Table I.

The choice of inflow velocities for the experiment involved balancing the higher signal-to-noise ratio from

higher inflow speeds against higher rotation rates (to maintain $\lambda$) that increased vibration in the turbine and support structure. We selected $0.8$ m/s for the 7-ply blades, which, as described later in this section, required an inflow speed of $0.55$ m/s for the 5-ply blades to maintain Cauchy similarity. To ensure that both tests were conducted in a Reynolds-number independent operational regime, water temperature was increased to $33^\circ$ C, decreasing viscosity.

Because the material properties of the carbon fiber and urethane are sensitive to temperature, $E$ for both blades was estimated through an in-water zero-inflow load test at $33^\circ$ C, the same water temperature used for the hydrodynamic tests. With the blade mounted on the turbine and positioned horizontally, calibration weights of 50-100 grams were incrementally added to the blade tip. With the addition of each weight, 3500 samples from the blade load cell recorded the applied force and a photograph was taken to determine the tip deflection and twist relative to the unloaded position (Fig. 6). The force and deflection measurements were then used to determine the bending stiffness, treating the blade as a cantilevered beam:

$$EI = \frac{FL^3}{3\delta.}, \tag{6}$$

where $I$ is the second moment of inertia, $F$ is the applied load, $L$ is the length of the cantilevered blade, and $\delta$ is the deflection at the blade tip. Fig 7(a,b) shows twist and deflection as a function of applied load. Because $I$ is a function of blade cross-section and constant for the two blades, a linear regression of the load-deflection response (Fig. 7(a)) can be used to estimate the ratio of the elastic moduli for the two blades as:

$$\frac{E_{5ply}}{E_{7ply}} = \frac{(EI)_{5ply}}{(EI)_{7ply}} = \frac{(F/\delta)_{5ply}}{(F/\delta)_{7ply}} = 0.47 \tag{7}$$

Consequently, to maintain $Ca$ similarity,

$$U_{5ply} = U_{7ply}\sqrt{\frac{E_{5ply}}{E_{7ply}}} = (0.8\mathrm{m/s})\sqrt{0.47} = 0.55\mathrm{m/s}. \tag{8}$$

The comparison of these experiments is carried out under the framework of the non-dimensional parameters for simultaneous hydrodynamic and hydroelastic scaling identified by Young [40]:

- Tip-speed ratio ($\lambda$): the same tip-speed ratio range, 2.5-8, is evaluated for the 5-ply and 7-ply blades
- Ratio of bending stiffness to torsional stiffness ($EI/GJ$) and bend-twist coupling ratio ($K_s/EI$): Having used the same material at the same fiber orientation for the 5-ply and 7-ply blades, we keep the ratio of effective bending to torsional stiffness and the bend-twist coupling equivalent, with only small variations expected from the use of semi-rigid polyurethane cast. Similarity in the bend-twist coupling is confirmed in Fig. 7(c).
- Froude number and Reynolds number: Froude number could not be matched between tests due to limitations on water height at our facility, and Reynolds number could not be matched due to sensitivity of the blade's material properties to temperature. To stay above Reynolds-independence at both flow speeds, water temperature was increased to the highest possible, 33°C. Changes in Froude and Reynolds number were not expected to have a significant effect on performance given that good agreement in $C_P$ and $C_T$ has been observed in prior experiments over similar flow conditions [44]. To verify low sensitivity to changes in $Fr$ and $Re$, we test a rigid blade with the same unloaded geometry at both flow conditions used for the 5-ply and 7-ply tests. The results are discussed in Sec. III.
- Density ratio ($\rho_s/\rho_f$): The density ratio between the solid composite blade and fluid varies between tests due to more polyurethane used in the 5-ply design, but since we are only concerned with scaling the steady-state hydrodynamic and hydroelastic behavior, we neglect density ratio for this study. Practically, up to 20% variation in material density would likely be sufficient even for modeling dynamic behavior [41].
- Cavitation number: Cavitation was not observed in either test case for the 5-ply and 7-ply blades and, thus, cavitation number was considered irrelevant to this experiment.
- Mach number: The turbine was operated in incompressible flow conditions and, thus, Mach number was also considered irrelevant in the context of hydrodynamics.

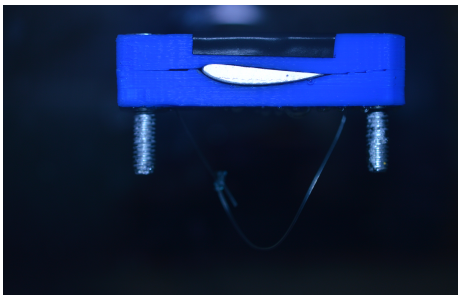

(a)

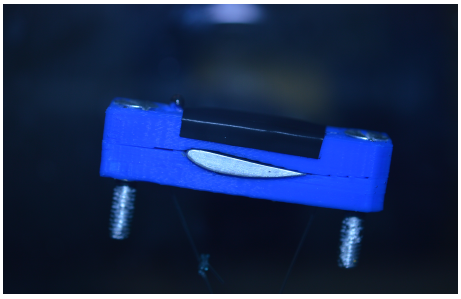

(b)

Fig. 6. For the in-water static test, deflection and twist are determined from photographs taken in the (a) unloaded and (b) loaded states.

In summary, physical limitations and assumptions lead us to hold constant four of the nine non-dimensional parameters governing rotor performance in this context: tip-speed ratio, bend-twist coupling ratio, bending to torsional stiffness, and Cauchy number.

TABLE I
MATERIAL PROPERTIES FOR HEXCEL AS4 CARBON FIBER.

| Material Property | Value |
|---|---|
| Longitudinal Young's modulus (parallel to fibers), $E_1$ | 115.56 GPa |
| Transverse Young's modulus (perpendicular to fibers), $E_2$ | 9.86 GPa |
| Shear modulus, $G_{12}$ | 4.826 GPa |
| Poisson's Ratio, $\nu_{12}$ | 0.335 |

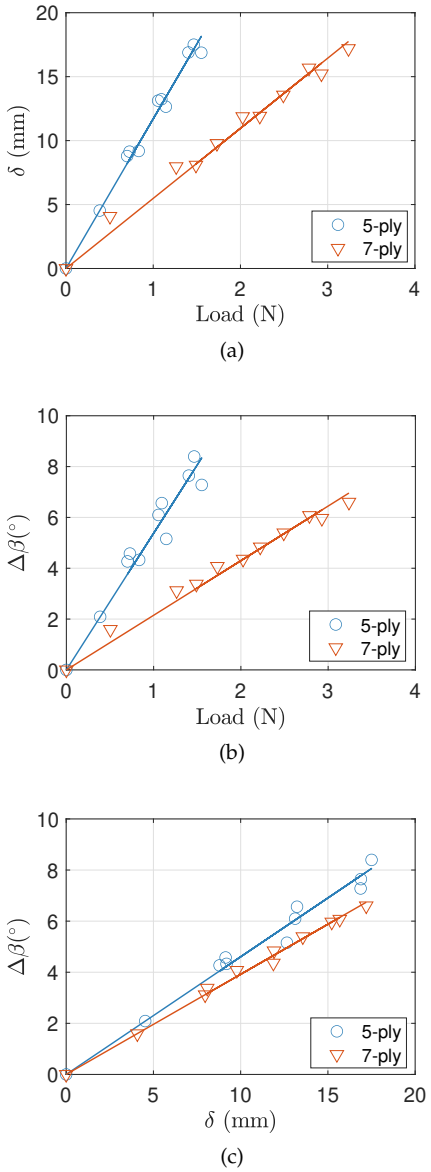


Fig. 7. (a) Deflection and (b) twist as a function of applied load for a 7-ply and 5-ply passive adaptive blade with the same 10° fiber orientation. Similarity in (c), twist as a function of deflection, is representative of the matching bend-twist coupling between blades.

Since our experiments are conducted in a relatively small channel, we note that blockage ratio is a relevant non-dimensional parameter, and was kept constant between both tests at 35%.

### G. Blade center of pressure

To support a comprehensive understanding of hydrodynamic and hydroelastic behavior of passive adaptive turbine blades, we approximate the span-wise and chord-wise center of pressure on the blade

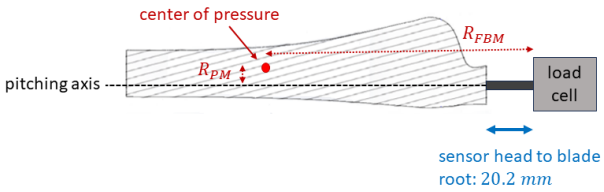


Fig. 8. Force and torque measured from the blade load cell are used to calculate the pitching moment arm, $R_{PM}$, and the flapwise bending moment arm, $R_{FBM}$. We further define $R_{PM}$ as the distance between the pitching axis and the chord-wise center of pressure, while $R_{FBM}$ is the distance between the sensor head of the blade load cell and the span-wise center of pressure.

using force and torque measurements from the six-axis load cell installed at the blade root. Referring to the coordinate system of the blade load cell defined in Fig. 4, we relate the pitching moment, $Q_{z,b}$, to the thrust force on the blade, $F_{y,b}$:

$$\langle Q_{z,b} \rangle = \langle F_{y,b} \rangle R_{PM}, \tag{9}$$

where $R_{PM}$ is the pitching moment arm, i.e., the chord-wise distance between the pitching axis (located at the quarter-chord) and the center of pressure on the blade (Fig. 8). $\langle Q_{z,b} \rangle$ and $\langle F_{y,b} \rangle$ are direct measurements from the blade load cell, averaged over the entire time series at each tip-speed ratio. We similarly relate the flapwise bending moment, $Q_{x,b}$, to the thrust force on the blade:

$$\langle Q_{x,b} \rangle = \langle F_{y,b} \rangle R_{FBM}, \tag{10}$$

where $R_{FBM}$ is the flapwise bending moment arm, i.e., the span-wise distance between the sensor head of the load cell and the center of pressure on the blade. Error in the center of pressure calculation is introduced through the span-wise variation in twist inherent to the blade geometry and the passive twist behavior observed during a test; Eqns 9 and 10 assume $F_{y,b}$ is perpendicular to the chord, which is an appropriate assumption for small changes in twist.

## III. RESULTS & DISCUSSION

Figures 9(a,b) show coefficients of performance and thrust for the 5-ply and 7-ply blade in inflow conditions corresponding to Cauchy similarity (Eqn. 5). Also shown is the performance of the 7-ply blade at the same inflow velocity as the 5-ply test, which demonstrates the sensitivity of blade performance to

a 50% change in Cauchy number. Figures 9(c,d) show deflection and twist at the blade tip as a function of tip-speed ratio. As hypothesized, we observe agreement between $C_T$, $\delta$, and $\Delta\beta$ when Cauchy similarity was maintained, particularly when flow is attached over the entire blade span ($\lambda > 4$), despite dissimilarity in Mach, Froude and density ratio, and for Reynolds numbers that are dissimilar but both within the asymptotic Reynolds-independent regime. More specifically, differences of 0-7% were observed in $C_T$, $\delta$, and $\Delta\beta$ compared to 50-65% for the 7-ply blade tested at 0.55 m/s and 0.8 m/s. In agreement with [41], our result demonstrates the effectiveness of using Cauchy number to scale passive adaptive marine current turbine blades and model their steady-state hydrodynamics and hydroelastics behaviors in a consistent, non-dimensional manner. Confidence in experimental application of scaling laws for passive adaptive blades broadens the impact of past and future lab-scale studies and encourages future work at similar scales, which is often financially accessible to a broader set of research groups.

Unexpectedly, we did not observe a collapse of $C_P$ between the 5-ply and 7-ply blades 9(a). Likely reasons for the disagreement include (1) differences in Reynolds and/or Froude number and (2) a surface defect in the 5-ply blade.

To understand the consequence of changing Reynolds and Froude numbers between 0.55 m/s and 0.80 m/s, we tested a rigid, aluminum blade with the same unloaded geometry at both flow conditions (Fig. 10). Over most tip-speed ratios, we observed minimal differences in $C_P$ of 3-8% and differences in $C_T$ of 3-5%. Disagreement over $3.5 < \lambda < 4.5$ is due to partial stall, where flow remains attached over part of the foil and bladespan, while agreement resumes over $\lambda < 3.5$ when the blade is in full stall. But for $\lambda > 4.5$, $C_P$ and $C_T$ are generally insensitive to changes in the Reynolds and Froude numbers. Because the differences in $C_P$ are small in comparison to the disagreement between the composite blades, we do not believe that the $C_P$ differences in the Cauchy similitude experiment can be attributed to variation in the Reynolds and/or Froude numbers. We hypothesize that the source of the disagreement in $C_P$ is a small (7 mm) surface defect in the urethane on the 5-ply blade near the mid-span and mid-chord of the blade. The defect, which created an uneven surface, may have caused early flow separation and, consequently, decreased power production, while having little effect on thrust. Future work will include repeating the experiments in this study to confirm this hypothesis.

Helpful to understanding the hydrodynamic and hydroelastic behavior shown in Fig. 9(a-d) are the center of pressure calculations summarized in Fig. 9(e,f). While the chord-wise center of pressure for symmetric foils is approximately at the quarter-chord ($x/c = 1/4$), Fig. 9(e) suggests continual variation for a deforming blade. We observe for $\lambda > 4$, the chord-wise center of pressure moves closer to the trailing edge as the tip-speed ratio increases. This same observation was made in a computational study of passive adaptive blade deformation by Zilic de Arcos, et al. [45]. Further, even for a rigid blade, we observe that the center of pressure moves closer to the trailing edge for the same tip-speed ratios (Fig. 9(e)). For a passive adaptive blade, this is likely the phenomenon that produces increased twist at high tip-speed ratios despite the observed decreases in deflection. Widely seen in studies of bend-twist coupled blades, an increase (or decrease) in deflection typically corresponds to an increase (or decrease) in twist [5] as loads are applied at a specified point on the blade. The result shown in Fig. 9 demonstrates that, in practice, the change in the center of pressure on the blade during turbine operation plays a large role in the observed hydrodynamic and hydroelastic behavior. Furthermore, Fig. 9(f) shows the span-wise center of pressure moving inward towards the blade root at increased tip-speed ratios. This aligns with our previous observations in that larger tip-speed ratios correspond to larger twist deformation and less power production and thrust. Given that the largest amount of twist (and load shedding) happens in the outer blade span, we would reasonably expect the center of pressure to move inward in cases with increased twist deformation. Conversely, we see that for the rigid blade with no blade deformation and higher power production and thrust, the span-wise center of pressure remains closer to the blade tip at high tip-speed ratios (Fig. 9(f)).

## IV. Conclusion

In this study, we conducted flume testing of a single-bladed turbine to explore the effectiveness of Cauchy-scaled passive adaptive blade experiments for modeling a blade's steady-state hydrodynamic and hydroelastic response. The main outcomes are as follows:

- When Cauchy similarity was met, some of the steady-state hydrodynamic and hydroelastic behavior (thrust coefficient, blade deflection, blade twist) was accurately modeled between scales. This outcome broadens the impact of previous lab-scale studies of passive adaptive blades and encourages future work at similar scales by increasing confidence in the experimental application of scaling laws.
- Moderate disagreement in the power coefficient was observed between tests, likely caused by a surface defect on the 5-ply blade.
- The chord-wise and span-wise centers of pressure varied across rotation rate and inflow velocity, significantly impacting blade deformation and corresponding hydrodynamic behavior.
- Rare for experimental turbine testing, we described methods for capturing blade deformation and the center of pressure on the blade during turbine operation which supports a broader understanding of passive adaptive blade behavior and their application in marine energy technology.

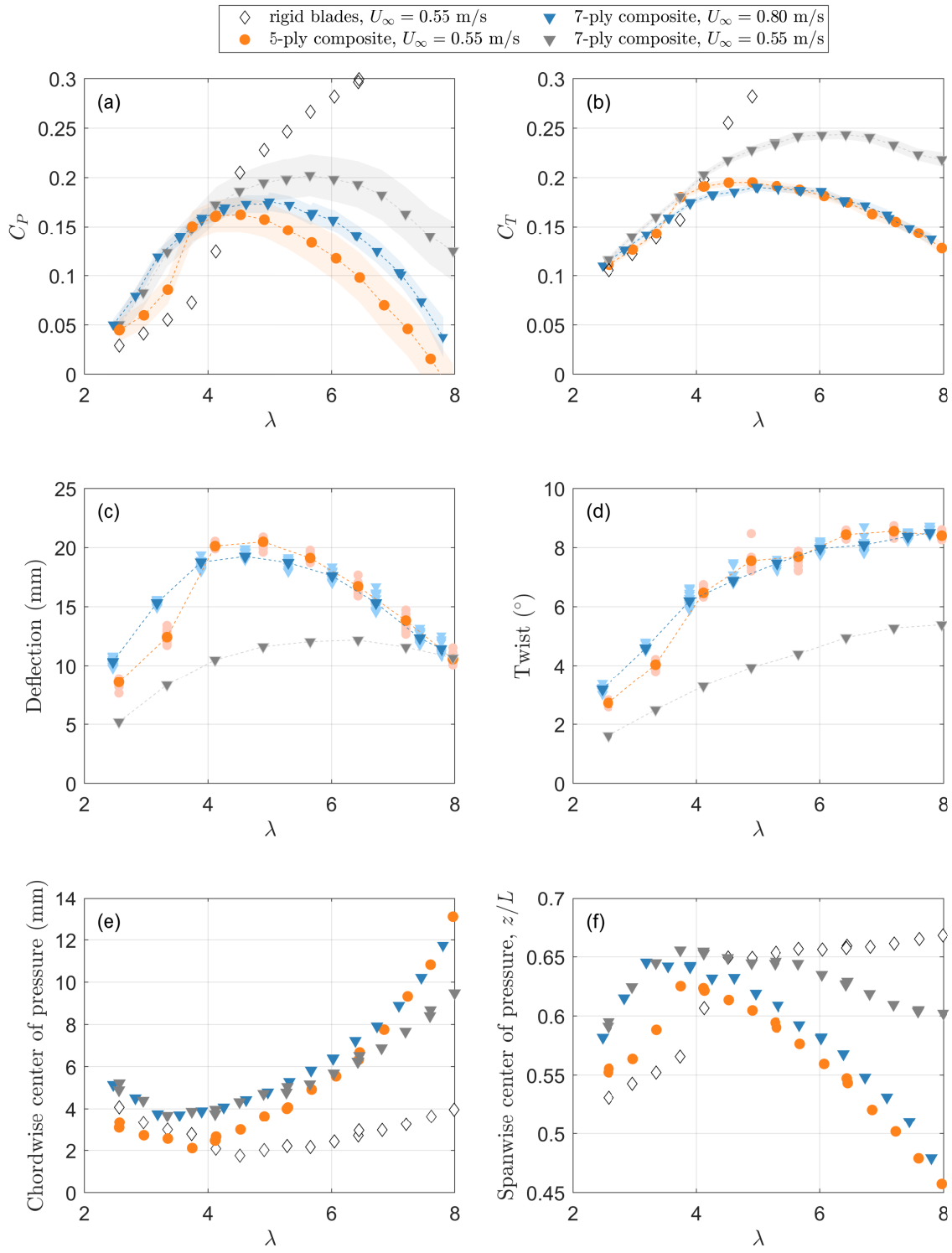


Fig. 9. Coefficients of (a) performance and (b) thrust as a function of tip speed ratio for a 7-ply and 5-ply composite blade in Cauchy-scaled flow conditions. The 7-ply blade is shown at both flow conditions to provide a reference. High-speed video of the passing blades provided measurements of (c) deflection and (d) blade twist at the tip as a function of tip-speed ratio. Shaded regions in (a,b) represent the interquartile range of measurements while the light orange and blue markers in (c,d) represent measurements from individual blade passages. The (e) chord-wise and (f) span-wise center of pressure are reported relative to the pitching axis and blade root, respectively. Positive values in (e) indicate a center of pressure closer towards the trailing edge of the blade. Position in (f) is normalized by the blade length, $L = 170$ mm, where $z/L = 0$ would indicate a center of pressure at the blade root and $z/L = 1$ would indicate a center of pressure located at the blade tip.

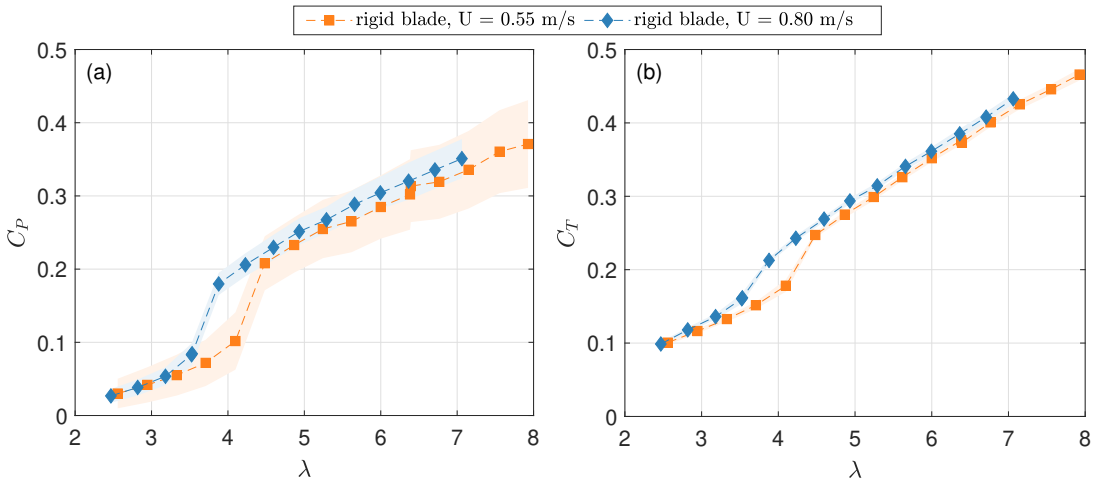


Fig. 10. Coefficients of (a) performance and (b) thrust as a function of tip-speed ratio for a rigid blade with the same unloaded geometry as the 5- and 7-ply composite blades. Shaded regions represent the interquartile range, which is smaller than the size of the markers in (b).

## APPENDIX

Blade geometry, where $r$ is the local radius, $R$ is the turbine radius, $c$ is the local chord, and $t$ is the local thickness:

| $r/R$ | $c/r$ | $t/c$ | Pre-Twist(°) |
|---|---|---|---|
| 0.244 | 0.318 | 1.000 | 14.60 |
| 0.262 | 0.303 | 1.000 | 14.60 |
| 0.300 | 0.271 | 0.963 | 14.60 |
| 0.330 | 0.484 | 0.350 | 14.56 |
| 0.355 | 0.554 | 0.223 | 14.02 |
| 0.381 | 0.499 | 0.208 | 13.01 |
| 0.410 | 0.438 | 0.201 | 11.46 |
| 0.441 | 0.385 | 0.193 | 10.03 |
| 0.474 | 0.334 | 0.185 | 9.32 |
| 0.510 | 0.288 | 0.177 | 8.48 |
| 0.548 | 0.247 | 0.167 | 7.81 |
| 0.590 | 0.212 | 0.167 | 7.05 |
| 0.635 | 0.183 | 0.159 | 6.25 |
| 0.684 | 0.159 | 0.147 | 5.69 |
| 0.736 | 0.140 | 0.147 | 5.21 |
| 0.790 | 0.126 | 0.148 | 4.66 |
| 0.902 | 0.106 | 0.149 | 3.66 |
| 0.959 | 0.100 | 0.150 | 3.17 |
| 1.000 | 0.096 | 0.154 | 3.31 |

## ACKNOWLEDGEMENT

We thank the Alice C. Tyler Charitable Trust for supporting the continued operation and development of the experimental facilities at the University of Washington. Additional thanks to Zachary Tully, Justin Burnett, Craig Hill, and Corey Crisp for their contributions to the lab-scale turbine, data acquisition system, and processing code.

## REFERENCES

[1] M. Motley and R. Barber, "Passive control of marine hydrokinetic turbine blades," *Composite Structures*, vol. 110, pp. 133–139, 2014.

[2] Y. Young and M. Motley, "Influence of material and loading uncertainties on the hydroelastic performance of advanced material propellers," in *Proceedings of the 2nd International Symposium on Marine Propulsors*, Hamburg, Germany, Jun. 2011.

[3] R. Nicholls-Lee, S. Turnock, and S. Boyd, "Application of bend–twist coupled blades for horizontal axis tidal turbines," *Renewable Energy*, vol. 50, pp. 541–550, 2013.

[4] R. Murray, T. Nevalainen, K. Gracie-Orr, D. Doman, M. Pegg, and C. Johnstone, "Passively adaptive tidal turbine blades: design tool development and initial verification," *International Journal of Marine Energy*, vol. 14, pp. 101–114, 2016.

[5] R. Barber, C. Hill, P. Babuska, R. Wiebe, A. Aliseda, and M. Motley, "Flume-scale testing of an adaptive pitch marine hydrokinertic turbine," *Composite Structures*, vol. 168, pp. 465–473, 2017.

[6] R. Murray, S. Ordonez-Sanchez, K. Porter, C. Johnstonre, D. Doman, and M. Pegg, "Towing tank and flume testing of passively adaptive composite tidal turbine blades," in *Proceedings of the European Wave and Tidal Energy Conference*, Cork, Ireland, 2017.

[7] K. Porter, S. Ordonez-Sanchez, R. Murray, M. Allmark, C. Johnstonre, T. O'Doherty, A. Mason-Jones, D. Doman, and M. Pegg, "Flume testing of passively adaptive composite tidal turbine blades under combined wave and current loading," *Journal of Fluids and Structures*, vol. 93, 2020.

[8] P. Jeffcoate, R. Starzmann, B. Elsaesser, S. Scholl, and S. Bischoff, "Field measurements of a full scale tidal turbine," *International Journal of Marine Energy*, vol. 12, pp. 3–20, 2015.

[9] A. Arredondo-Galeana, A. Young, A. Smyth, and I. Viola, "Unsteady load mitigation through a passive trailing-edge flap," *Journal of Fluids and Structures*, vol. 106, 2021.

[10] Y. Young, N. Garg, P. Brandner, B. Pearce, D. Butler, D. Clarke, and A. Phillips, "Load-dependent bend-twist coupling effects on the steady-state hydroelastic response of composite hydrofoils," *Composite Structures*, vol. 189, pp. 398–418, 2018.

[11] G. Zarruk, P. Brandner, B. Pearce, and A. Phillips, "Experimental study of the steady fluid–structure interaction of flexible hydrofoils," *Journal of Fluids and Structures*, vol. 51, pp. 326–343, 2014.

[12] H. Wada, H. Murayama, Y. Minami, H. Uzama, and K. Kageyama, "Deformation evaluation of elastic composite blade models for a tidal power generation by fluid-structure interaction analysis," in *Proceedings of the 18th International Conference on Composite Materials*, Jeju, Korea, Aug. 2011.

[13] G. Pisetta, R. Le Mestre, and I. Viola, "Morphing blades for tidal turbines: A theoretical study," *Renewable Energy*, vol. 183, pp. 802–819, 2022.

[14] A. Lee and R. Flay, "Compliant blades for passive power control of wind turbines," *Wind Engineering*, vol. 24, no. 2, pp. 3–11, 2000.

[15] D. Lobitz and P. Veers, "Load mitigation with bending/twist-coupled blades on rotors using modern control strategies," *Wind Energy*, vol. 6, no. 2, pp. 105–117, 2002.

[16] Y. Young, "Fluid–structure interaction analysis of flexible composite marine propellers," *Journal of Fluids and Structures*, vol. 24, no. 6, pp. 799–818, 2008.

[17] S. Gowing, P. Coffin, and C. Dai, "Hydrofoil cavitation improvements with elastically coupled composite materials," in *Proceedings of the 25th American Towing Tank Conference*, Iowa City, IA, USA, 1998.

[18] J. Blasques, C. Berggreen, and P. Andersen, "Hydro-elastic analysis and optimization of a composite marine propeller," *Marine Structures*, vol. 23, no. 1, pp. 22–38, 2010.

[19] S. Heinzen, J. Hall, C.E., and A. Gopalarathnam, "Development and testing of a passive variable-pitch propeller," *Journal of Aircraft*, vol. 52, no. 3, pp. 748–763, 2015.

[20] Y. Young, M. Motley, R. Barber, E. Chae, and N. Garg, "Adaptive composite marine propulsors and turbines: progress and challenges," *Applied Mechanics Review*, vol. 68, no. 6, 2016.
[21] N. Karaolis, P. Musgrove, and G. Jeronimidis, "Active and passive aerodynamic power control using asymmetric fibre reinforced laminates for wind turbine blades," in *Proceedings of the 10th British Wind Energy Association Conference*, D. Milbrow, Ed., London, England, Mar. 1988.
[22] R. van den Berg, P. Joosse, and B. Visser, "Passive power control by self twisting blades," in *Proceedings of the European Wind Energy Association Conference and Exhibition*, Thessaloniki, Greece, Oct. 1994.
[23] C. Bottasso, F. Campagnolo, A. Croce, and C. Tibaldi, "Optimization-based study of bend–twist coupled rotor blades for passive and integrated passive/active load alleviation," *Wind Energy*, vol. 16, no. 8, pp. 1149–1166, 2013.
[24] D. Lobitz and P. Veers, "Aeroelastic behavior of twist-coupled hawt blades," in *ASME Wind Energy Symposium*, Reno, NV, USA, Jan. 1998.
[25] L. Wang, L. Xiongwei, and A. Kolios, "State of the art in the aeroelasticity of wind turbine blades: aeroelastic modelling," *Renewable and Sustainable Energy Reviews*, vol. 64, pp. 195–210, 2016.
[26] P. Berring, K. Branner, C. Berggreen, and H. Knudsen, "Torsional performance of wind turbine blades-part 1: experimental investigation," in *Proceedings of the 16th International Conference on Composite Materials*, Kyoto, Japan, 2007.
[27] S. Barr and J. Jaworksi, "Optimization of tow-steered composite wind turbine blades for static aeroelastic performance," *Renewable Energy*, vol. 139, pp. 859–872, 2019.
[28] C. Ong and S. Tsai, "Elastic tailoring of a composite d-spar," Sandia National Laboratories, Tech. Rep., 1998, report No: SAND98-1750.
[29] D. Griffith and T. Ashwill, "The sandia 100-meter all-glass baseline wind turbine blade," Sandia National Laboratories, Tech. Rep., 2011, report No: SNL100-00.
[30] F. Campagnolo, C. Bottasso, and P. Bettini, "Design, manufacturing and characterization of aero-elastically scaled wind turbine blades for testing active and passive load alleviation techniques within a abl wind tunnel," *Journal of Physics: Conference Series*, vol. 524, 2014.
[31] A. Mason-Jones, D. O'Doherty, C. Morris, T. O'Doherty, C. Byrne, P. Prickett, R. Grosvenor, I. Owen, S. Tedds, and R. Poole, "Non-dimensional scaling of tidal stream turbines," *Energy*, vol. 44, no. 1, pp. 820–829, 2012.
[32] C. Bottasso, F. Campagnolo, and V. Petrovic, "Wind tunnel testing of scaled wind turbine models: Beyond aerodynamics," *Journal of Wind Engineering and Industrial Aerodynamics*, vol. 127, pp. 11–28, 2014.
[33] P. Friedmann, "Aeroelastic scaling for rotary-wing aircraft with applications," *Journal of Fluids and Structures*, vol. 19, no. 5, pp. 635–650, 2004.
[34] C. Wolowicz, J. Bowman, and J. Gilbert, W.P., "Similitude requirements and scaling relationships as applied to model testing," NASA, Tech. Rep., 1979, technical Paper 1435.
[35] Z. Wan and C. Cesnik, "Geometrically nonlinear aeroelastic scaling for very flexible aircraft," *AIAA Journal*, vol. 52, no. 10, 2014.
[36] S. Chakrabarti, *The Theory and Practice of Hydrodynamics and Vibration*. World Scientific, 2002.
[37] S. Hughes, *Physical models and laboratory techniques in coastal engineering*. World Scientific, 1993.
[38] M. Motley and Y. Young, "Scaling of the transient hydroelastic response and failure mechanisms of self-adaptive composite marine propellers," *Internation Journal of Rotating Machinery*, vol. 2012, 2012.
[39] Y. Young, C. Harwood, F. Montero, J. Ward, and S. Ceccio, "Ventilation of lifting bodies: Review of the physics and discussion of scaling effects," *Applied Mechanics Reviews*, vol. 69, no. 1, 2017.
[40] Y. Young, "Dynamic hydroelastic scaling of self-adaptive composite marine rotors," *Composite Structures*, vol. 92, pp. 96–106, 2010.
[41] G. Ng, A. Vishneek, J. Martins, and Y. Young, "Scaling the dynamic response and stability of composite hydrodynamic lifting surfaces," *Composite Structures*, vol. 285, 2022.
[42] K. Cox and A. Echtermeyer, "Structural design and analysis of a 10mw wind turbine blade," *Energy Procedia*, vol. 25, pp. 194–201, 2012.
[43] R. Murray, K. Gracie-Orr, D. Doman, M. Pegg, and C. Johnstone, "Design of a passively adaptive rotor blade for optimized performance of a horizontal-axis tidal turbine," in *Proceedings of the 10th European Wave and Tidal Energy Conference*, Aalborg, Denmark, Aug. 2013.
[44] K. Van Ness, C. Hill, J. Burnett, A. Aliseda, and B. Polagye, "Experimental comparison of speed and pitch control strategies for horizontal-axis current turbines," *Journal of Ocean Engineering and Marine Energy*, vol. 7, pp. 83–96, 2020.
[45] F. Zilic de Arcos, C. Vogel, and H. Willden, "Hydrodynamic independence and passive control application of twist and flapwise deformations of tidal turbine blades," *Journal of Fluids and Structures*, vol. 118, 2023.